Pergamon

Int. J. Heat Mass Transfer. Vol. 38, No. 3, pp. 495–501, 1995

0017-9310/95 $9.50+0.00

0017-9310(94)00177-4

Numerical investigation of turbulent flows and heat transfer in a rib-roughened channel with longitudinal vortex generators†

J. X. ZHU,‡ M. FIEBIG and N. K. MITRA§

Institut für Thermo- und Fluiddynamik, Ruhr-Universität Bochum, Postfach 102148, 44721 Bochum, Germany

(*Received* 31 *January* 1994 *and in final form* 1 *June* 1994)

Abstract—Three-dimensional turbulent flows and heat transfer in a rectangular channel with longitudinal vortex generators on one wall and rib-roughness elements on the other wall have been modeled by the k–ε model and law of the wall and computed. Rectangular winglets have been used as vortex generators. Results show that the combined effect of rib-roughness and vortex generators can enhance the average Nusselt number by nearly 450%.

1. INTRODUCTION

Heat transfer enhancement in turbulent channel flows in plate heat exchangers can be achieved by introducing artificial surface roughness such as ribs on the wall [1, 2]. For small ratios of rib height to the channel height, the heat transfer and friction characteristics of the rib-roughened surface can be modeled by the semi-empirical law of the wall for rough surfaces. An alternative method for heat transfer enhancement in laminar as well as turbulent channel flows is the introduction of fins to increase the heat transfer surface area. The increase in heat transfer by increasing fin surface is limited from the economical consideration. However, if the fins are selected in the form of longitudinal vortex generators (VGs), then the additional heat transfer benefit coming from the churning of the flow may exceed the benefit of increasing the heat transfer surface by fins. Figure 1 shows four basic forms of wing-type longitudinal vortex generators—delta wing, rectangular wing and the corresponding winglet pairs. These triangular or rectangular pieces can be mounted on the wall with an angle of attack β to the main flow direction. Longitudinal vortices are generated along their side edges by separation of the flow due to the pressure difference between the upstream and downstream side of the VG. These vortices rotate the flow around the main flow direction, see Fig. 2. They enhance mixing of the fluids close to and far from the wall.

Systematic experimental and numerical investigations on the influence of wing-type vortex generators (Fig. 1) on flow losses and heat transfer were reported by the present group [3–7]. The experimental investigations were carried out in transition and turbulent regimes [3, 4] for Reynolds numbers between 2000 and 8000, and numerical investigations were carried out in laminar [5] and turbulent regimes [6, 7].

The experiments were performed by measuring the local heat transfer on the bottom plate of a rectangular channel. The vortex generators were mounted also on the bottom plate. The experimental investigations showed that one wing or a winglet pair could cause a local increase of heat transfer by several hundred percent, and an average increase of 50% or more on a wall area which was 50 times the VG area. The rectangular winglets gave the largest heat transfer enhancement for an angle of attack, β, of around 45°.

Numerical simulations of turbulent flows in a rectangular channel with mounted VGs on the bottom wall were carried out by Zhu *et al.* [6, 7]. The flow field was calculated by solving Reynolds-averaged Navier–Stokes and energy equations, and the turbulence was taken into account by solving standard k–ε model equations with wall law. A comparison [6] of the numerical results with the available experimental results of Pauley and Eaton [8] showed that the k–ε model could simulate flow with embedded longitudinal vortices accurately except in the vortex core, where a disagreement of 13% might appear.

Computations were also performed for a channel with the ratio the winglet height to the channel height $h/H = 0.6$ and the Reynolds number $Re = 50\,000$. Results showed that the VGs on the lower wall could have substantial effects on heat transfer on the upper wall without VG, especially when rectangular winglets were used and when the channel height H was slightly larger than the projected height h of the VG, see Fig. 3b.

The vortex generators on one wall can increase the

†Dedicated to Professor Dr -Ing H. Unger on the occasion of his 60th birthday.

‡Autokühlergesellschaft, Hofgeismer, Germany.

§Author to whom correspondence should be addressed.

NOMENCLATURE

A	Von Driest's constant
A_L	channel wall area
A_w	winglet surface area
B	channel width
C_1, C_2	constants in k–ε model
C_μ	constants in k–ε model
c_P	specific heat at constant pressure
D_h	hydraulic diameter
E	constant in logarithmic law of the wall
e	rib height
e^+	nondimensional rib height, see equation (19)
f	apparent friction factor
f_0	apparent friction factor for a plane channel
G	production of turbulence kinetic energy
$\bar{G}$	see equations (16) and (18)
H	channel height
i, j	see equation (18)
k	turbulence kinetic energy
L	length of a periodic element of the channel
Nu	Nusselt number
P	see equation (14)
p	static pressure
Pr	Prandtl number
Pr_t	turbulent Prandtl number
q_w	wall heat flux
R	see equations (16) and (17)
Re	Reynolds number
Re_{Dh}	Reynolds number based on hydraulic diameter and maximum velocity
r	rib pitch
s	see Fig. 3b
t	time
T	temperature
T_b	bulk temperature
T_p	temperature at the grid point adjacent to wall
T_w	wall temperature
U_{max}	streamwise maximum velocity
U_j	jth velocity component
u_m	average axial velocity
u, v, w	velocity components
x_j	cartesian coordinates
x, y, z	cartesian coordinates
y^+	wall coordinate.

Greek symbols

β	angle of attack of vortex generators
Γ	thermal diffusivity
Γ_t	turbulent thermal diffusivity
γ	see equation (17)
δ	Kronecker delta
ε	dissipation rate of turbulence energy
ϑ	dimensionless temperature
κ	von Karman constant
λ	thermal conductivity
μ	molecular viscosity
μ_t	turbulent viscosity
ρ	density
$\sigma_k, \sigma_\varepsilon$	turbulent "Prandtl number" for diffusion of k and ε
ϕ	dependent variable, see equation (9)
τ_w	wall shear stress.

average heat transfer by nearly 30% at the cost of large flow losses (nearly 20 times) in comparison to a channel without VGs. Hence, putting VGs on both wall will be impractical on account of flow losses. Of course these results depend strongly on the h/H ratio. One interesting way to increase heat transfer further is to mount VGs on one wall and artificial surface roughness such as ribs on the other wall. Since rectangular winglets increase heat transfer on the opposite wall [9], in a channel configuration with one

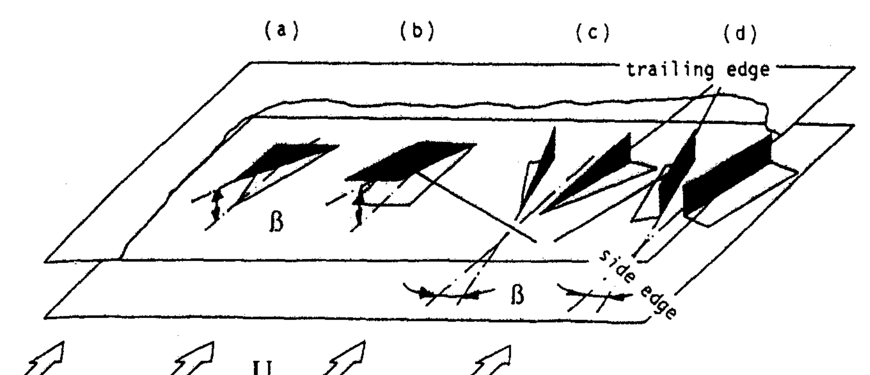

Fig. 1. Different forms of wing-type vortex generators; (a) delta wing, (b) rectangular wing, (c) delta winglet pair, (d) rectangular winglet pair; β, angle of attack.

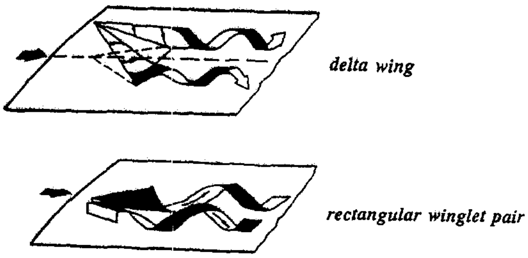

Fig. 2. Schematic of longitudinal vortex generator behind a delta wing and a rectangular winglet pair.

adiabatic wall and an isothermal wall, rectangular winglets can be mounted on the adiabatic wall and roughness elements on the isothermal wall. The combined effects of rib-roughened wall and the longitudinal vortices on the heat transfer in a turbulent channel flow have never been reported.

The purpose of the present work is numerical modeling and simulation of three-dimensional turbulent flows in a rectangular channel. One wall of the channel contains rows of longitudinal vortex generators in the form of rectangular winglets, and the opposite wall contains distributed ribs. Flow structure and heat transfer shall be analyzed. The present study has industrial applications. For example, the flame protection shrouds of industrial burners are often cooled by preheating air flowing through an annulus whose outer side is adiabatic.

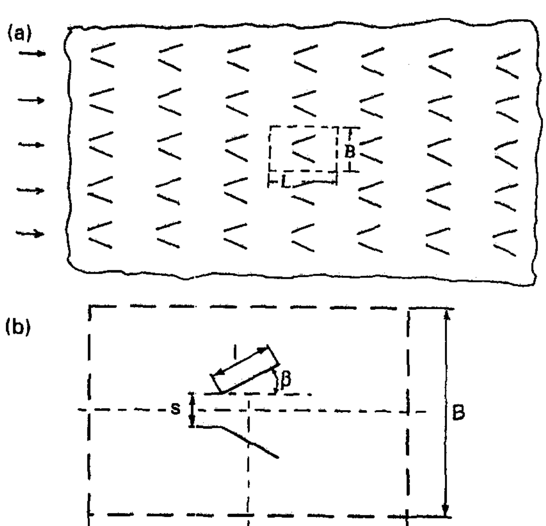

Fig. 3. (a) Schematic of a parallel wall channel with a series of vortex generators mounted on one channel wall (overview). (b) One element in the periodically fully developed region of the arrangement shown in (a).

2. FLOW MODELING AND METHOD OF SOLUTION

2.1. *Geometry*

The turbulent flow is considered in a rectangular channel (e.g. between two parallel plates of a finned-plate heat exchanger). One plate (henceforth the bottom plate) is finned. The fins are rows of mounted longitudinal vortex generators in the form of rectangular pairs of winglets, see Fig. 3a. The top plate is smooth or rib-roughened. In order to reduce the computational time, the flow in the channel is considered periodically fully developed so that the flow need be computed only in one periodic element of length L and width B, see Fig. 3a and b. Figure 3b is the computational domain. Symmetry is assumed at $B/2$ so that computation needs to be performed only in half of the channel width. The rib height is e and rib pitch is r.

2.2. *Basic equations*

The flow in the channel is described by the three-dimensional Reynolds-averaged Navier–Stokes and energy equations for an incompressible medium. Turbulence is modeled by the standard k–ε model of Launder and Spalding [10]. The equations are written in cartesian tensor form as [7]:

continuity

$$\frac{\partial U_i}{\partial x_i} = 0 \tag{1}$$

momentum

$$\rho\frac{\mathrm{D}U_j}{\mathrm{D}t} = -\frac{\partial p}{\partial x_j} + \frac{\partial}{\partial x_i}\left[(\mu+\mu_t)\left(\frac{\partial U_i}{\partial x_j}+\frac{\partial U_j}{\partial x_i}\right)-\frac{2}{3}\rho k\delta_{i,j}\right] \tag{2}$$

energy

$$\rho\frac{\mathrm{D}T}{\mathrm{D}t} = \frac{\partial}{\partial x_i}\left[(\Gamma+\Gamma_t)\frac{\partial T}{\partial x_i}\right] \tag{3}$$

where the turbulent viscosity μ_t and the turbulent dynamic thermal diffusivity Γ_t are given by

$$\mu_t = c_\mu \rho k^2/\varepsilon \tag{4}$$

$$\Gamma_t = \frac{\mu_t}{Pr_t}. \tag{5}$$

The turbulence kinetic energy k and its dissipation rate ε are computed from the standard k–ε model of Launder and Spalding [10]:

$$\rho\frac{\mathrm{D}k}{\mathrm{D}t} = \frac{\partial}{\partial x_i}\left(\frac{\mu_t}{\sigma_k}\frac{\partial k}{\partial x_i}\right)+G-\rho\varepsilon \tag{6}$$

$$\rho\frac{\mathrm{D}\varepsilon}{\mathrm{D}t} = \frac{\partial}{\partial x_i}\left(\frac{\mu_t}{\sigma_\varepsilon}\frac{\partial \varepsilon}{\partial x_i}\right)+c_1\frac{\varepsilon}{k}G-c_2\rho\frac{\varepsilon^2}{k}. \tag{7}$$

G denotes the production rate of k and is given by

$$G = \mu_t \left(\frac{\partial U_i}{\partial x_j} + \frac{\partial U_j}{\partial x_i}\right)\frac{\partial U_i}{\partial x_j}. \quad (8)$$

The standard constants are employed,

$$c_\mu = 0.09, \quad c_1 = 1.44, \quad c_2 = 1.92$$

$$\sigma_k = 1.0, \quad \sigma_\varepsilon = 1.3, \quad Pr_t = 0.9.$$

2.3. *Boundary conditions*

Since we compute only in a periodic element, the following periodicity conditions are used in the inlet and exit

$$\phi(x,y,z) = \phi(x+L,y,z) \quad (9)$$

where

$$\phi = \{u, v, w, \kappa, \varepsilon, \theta\}$$

and

$$\theta(x,y,z) = \frac{T(x,y,z)-T_w}{T_b(x)-T_w} \quad (10)$$

where T_b is the bulk temperature. The velocity components u, v and w are zero on the solid walls. The lower wall with rectangular winglet is adiabatic. The upper wall is isothermal, $T_w =$ const.

The upper wall is either smooth or rib-roughened. For the smooth wall we use the following wall function of Launder and Spalding [10]:

$$\tau_w = \frac{\delta u_p c_\mu^{1/4} k_p^{1/2} \kappa}{\ln(Ey^+)} \quad (11)$$

where

$$y^+ = \frac{\rho y_p c_\mu^{1/4} k_p^{1/2}}{\mu} \quad (12)$$

and $\kappa = 0.42$, $E = 9.0$. The subscript p refers to the grid point adjacent to the wall. For the temperature boundary condition, the wall heat flux is derived from the thermal wall function [10]:

$$q_w = \frac{(T_w - T_p)\rho c_p c_\mu^{1/4} k_p^{1/2}}{Pr_t\left[\frac{1}{\kappa}\ln(Ey^+) + P\right]} \quad (13)$$

where the empirial function P is given by

$$P = \frac{\pi/4}{\sin(\pi/4)}\left(\frac{A}{\kappa}\right)^{1/2}\left(\frac{Pr}{Pr_t} - 1\right)\left(\frac{Pr_t}{Pr}\right)^{1/4}. \quad (14)$$

For the rib-roughened wall we use the wall functions of Hanjalic and Launder [11] and Donne and Meyer [12]:

$$u_p = \sqrt{\tau_w/\rho}\left[\frac{1}{\kappa}\ln\left(\frac{y_p}{e}\right) + R\right] \quad (15)$$

$$\frac{(T_p - T_w)\rho c_p u_c}{q_w} = \frac{Pr_t}{\kappa}\ln\left(\frac{y_p}{e}\right) + \bar{G} \quad (16)$$

where R and G are obtained from Han *et al.* [2],

$$R = 4.9\left(\frac{45°}{\gamma}\right)^{0.57}\left(\frac{r/e}{10}\right)^n \quad (17)$$

with

$$n = -0.13 \quad \text{for} \quad r/e \leqslant 10$$

$$n = 0.53\left(\frac{\gamma}{90°}\right)^{0.71} \quad \text{for} \quad r/e \geqslant 10.$$

Here γ is the angle of incidence of the roughness elements to the main flow direction,

$$\bar{G} = 8\left(\frac{e^+}{35}\right)^i \bigg/ \left(\frac{\gamma}{45°}\right)^j \quad (18)$$

with

$$e^+ = eu_\tau/v \quad (19)$$

and

$$i = 0 \quad \text{for} \quad e^+ < 35$$

$$i = 0.28 \quad \text{for} \quad e^+ \geqslant 35$$

$$j = 0.5 \quad \text{for} \quad \gamma < 45°$$

$$j = -0.45 \quad \text{for} \quad \gamma \geqslant 45°.$$

2.4. *Method of solution*

A numerical scheme based on the SOLA-algorithm [13] was modified by the authors' group for the computation of the turbulent flows in a rectangular channel with vortex generators [9]. The SOLA-algorithm solves the time-dependent Navier–Stokes equations directly for the primitive variables by advancing the solution explicitly in time. Steady-state solution is obtained when time gradients become negligibly small. Details of this scheme can be found in ref. [7]. For the cases considered here, we obtained only steady solutions. From the computed velocity and temperature fields, apparent friction factor f and the local Nusselt number Nu on the channel wall were calculated by using the following equations:

$$f = \frac{H}{L}\frac{p_1 - p_2}{\rho u_m^2} \quad (20)$$

$$Nu = \frac{q_w D_h}{\lambda(T_w - T_b)}. \quad (21)$$

Here L is the length of the computational domain (i.e. the length of the periodic element), u_m is the average axial velocity, ρ is the density and p_1 and p_2 are the static pressures at the inlet and exit, respectively. Although p_1 and p_2 depend on the location (y, z), the difference $(p_1 - p_2)$ is the same at every (y, z) location. This follows from the periodicity condition. The local Nusselt number Nu can be averaged on the channel in order to obtain the average Nusselt number $\overline{Nu}$. In equation (21) q_w is the local heat flux, D_h the hydraulic diameter, T_b the local bulk temperature, T_w the wall temperature and λ the heat conductivity. As a reference case, fully developed turbulent flow and heat

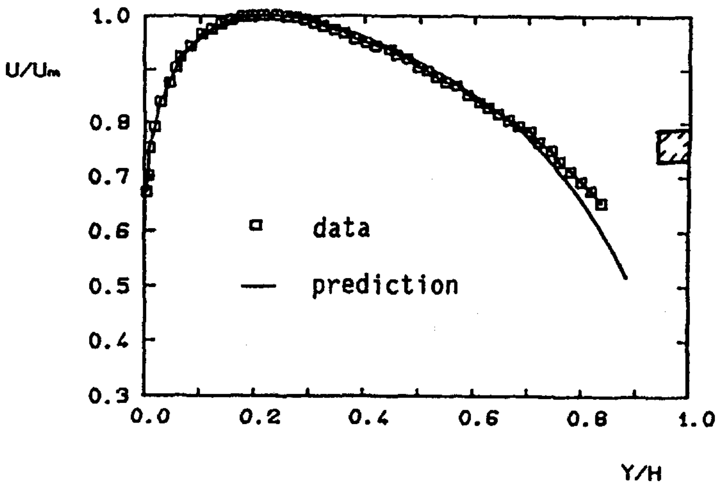

Fig. 4. Comparison between our numerical results and experimental data from ref. [9]. Mean velocity profile in a parallel wall channel with one smooth channel wall and one rib-roughened channel wall. $Re_H = 111\,200$, $e/H = 0.059$, $r/e = 10$.

transfer were also computed in a smooth plane channel. The Nusselt number and the apparent friction factor for a smooth channel were denoted as Nu_0 and f_0, respectively.

3. RESULTS AND DISCUSSION

3.1. *Validation of computations*

Before we investigated the combined effect of vortex generator and roughness elements, we had tested the computational scheme by computing the flow in a smooth two-dimensional channel with one isothermal and one adiabatic wall. The Reynolds number based on the hydraulic diameter was 3×10^5. Fully developed turbulent flow was calculated iteratively by enforcing periodicity boundary conditions, see equations (9) and (10), in a channel of length $2H$ and height H on 60×50 grids. The computed apparent friction factor f and the Nusselt number Nu differ from the values given in the literature [14] by 2% and 3.8%, respectively. A second test case of a fully developed asymmetric flow in a plane channel with one rib-roughened wall was computed and the results were compared with the measurements of Hanjalic and Launder [11]. The channel has a length $L = 3700$ mm, height $H = 54$ mm, pitch of the roughness elements (ribs) $r = 31.8$ mm and height of the ribs $e = 3.18$ mm. The computations were carried out in a periodic element with periodicity boundary conditions on a grid of 60×15. The Reynolds number Re_H based on the channel height and the maximum velocity U_{max} is 112 000.

Figure 4 shows excellent agreement of the computed normalized fully developed axial velocity with the experimental results of Hanjalic and Launder [11].

Comparisons of numerical simulations of longitudinal vortex embedded in the boundary layer of a channel wall with available experimental results have been presented in ref. [6]. Results showed that the k–ε model can adequately describe the flow with longitudinal vortices, except at the vortex core where the numerical results can deviate from the experimental results by nearly 13%.

Further computations were carried out in order to investigate separately the influence of the roughness elements, influence of rectangular winglets and the combined effect of roughness elements and vortex generators.

3.2. *Influence of roughness elements on heat transfer and flow loss*

Computations were carried out for a two-dimensional channel with a smooth adiabatic and a rib-roughened isothermal wall. The Reynolds number based on the hydraulic diameter Re_{Dh} is 3×10^5. The dimensionless rib height is $e/H = 0.03$ and the rib pitch $r/e = 10$. The results show the following increase in average Nusselt number $\overline{Nu}$ and f:

$$\frac{\overline{Nu}}{Nu_0} = 2.1 \quad \text{and} \quad \frac{f}{f_0} = 3.59.$$

It should be noted here that rib roughness on both walls has not been considered, since ribs on the adiabatic wall will possibly have negligible effects on heat transfer on the other wall.

3.3. *Influence of rows of rectangular winglets on one wall on heat transfer*

For this case the other wall was treated as smooth. The following data were used (see Fig. 5): $Re_{Dh} = 3 \times 10^5$, $l = 1.2H$, $h = 0.6H$, $s = 3.75H$, $B = 4H$, $L = 2.5H$, $3.75H$, $5H$ for $\beta = 45°$ and $L = 3.75H$ with $\beta = 15°$, $25°$, $35°$ and $45°$, $Pr = 0.7$. Table 1 presents the results for $\beta = 45°$.

Here A_L is channel wall area and A_w is the wing

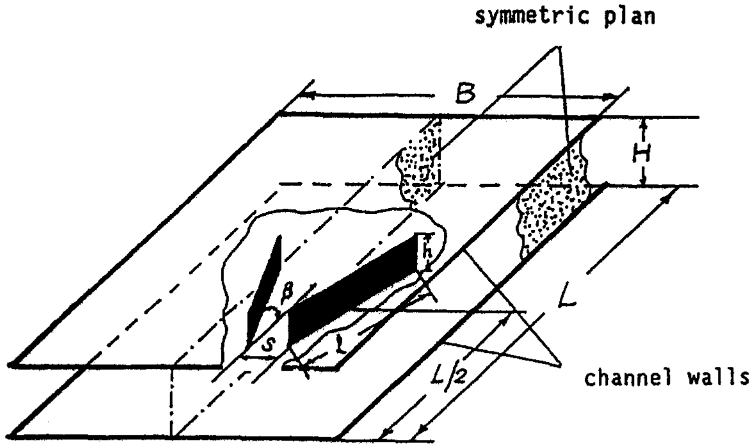

Fig. 5. Computational domain and geometrical parameters.

Table 1. Influence of period length on the average Nusselt number $\overline{Nu}$ for $\beta = 45°$ and flow loss, $Re_{Dh} = 3 \times 10^5$

L/H	2.5	3.75	5
A_L/A_w	7	10.4	44.0
$\overline{Nu}/Nu_0$	3.8	3.41	2.9
f/f_0	43.2	32	25.5
P_{ROC}/P_{RO}	98.4	67.8	38.9

Table 3. Influence of Reynolds number on Nusselt number and flow loss, RWP, $\beta = 45°$, $L = 3.75H$, $h = 0.64H$, $l = 1.2H$, $Pr = 0.7$

$Re \times 10^{-4}$	2.5	5.0	10	15
$\overline{Nu}/Nu_0$	2.90	3.34	3.42	3.41
f/f_0	22.5	26.2	30.3	32.0
P_{ROC}/P_{RO}	38.9	63.2	68.5	67.8
Nu_0	99	145	253	351.3

surface area. P_R is the flow loss, defined as

$$P_R = \Delta p\, u_m B H \tag{22}$$

and P_{RO} is the flow loss for the reference case (i.e. plane channel). P_{ROC} is the flow loss for a plane channel (without winglet) for the case when the $\overline{Nu}$ is same as that for the channel with winglet, and the enhancement is obtained by increasing only the Reynolds number. To estimate P_{ROC} we used the following correlations for a plane channel, as given by Sparrow *et al.* [15] and Kakac *et al.* [14]:

$$Nu = 0.023 Re_{Dh}^{0.8}\, Pr^{0.4} \tag{23}$$

$$f = 0.0868 Re_{Dh}^{-1/4}. \tag{24}$$

Table 1 shows that the increase in flow loss is much larger than the enhancement in $\overline{Nu}$ when vortex generators are used. However, such enhancement without the use of vortex generators may cause twice as much flow loss as with vortex generators. Table 2 shows the influence of the angle of attack β on the Nu, f and P_{ROC}.

Tables 1 and 2 show that a large Nu can be obtained by using small period length (i.e. densely packed vortex generators) and a large angle of attack. Table 2 also shows that the friction factor increases faster than $\overline{Nu}$ as β increases.

Table 3 presents the effect of Reynolds number on heat transfer and flow loss for the flow in a smooth channel with vortex generators. As is expected, both heat transfer and flow loss increase with Re. However, the increase in $\overline{Nu}$ is nearly linear ($\overline{Nu} \approx Re^{0.8}$), whereas the increase in f is much faster ($f \approx Re^{2.75}$).

Table 4 shows the effect of the Prandtl number Pr on heat transfer. With increasing Pr, the Nusselt number, Nu_0, in a plane channel increases steeply. In contrast, the enhancement due to the vortex generators ($\overline{Nu}/Nu_0$) decreases with increasing Pr. This is also reflected in the decreasing P_{ROC}/P_{RO} values with increasing Pr.

Table 2. Influence of angle of attack β, rectangular winglet pair (RWP) $L = 3.75H$, $h = 0.6H$, $l = 1.2H$, $Pr = 0.7$, $Re = 1.5 \times 10^5$

β	15°	25°	35°	45°
$\overline{Nu}/Nu_0$	2.43	2.59	3.04	3.41
$Nu_0 = 351.3$				
f/f_0	6.16	10.9	18.6	32
P_{ROC}/P_{RO}	21.2	26.4	45.7	67.8

3.4. *Combined effect vortex generators and wall roughness*

Table 5 presents the combined effect of rib-roughness and rectangular winglets.

Comparison of Tables 1, 2 and 5 show that, for a channel with an adiabatic and an isothermal wall, the combination of rib roughness and winglets produces appreciable heat transfer enhancement. More than 450% enhancement of the Nusselt number is possible.

Table 4. Influence of the Prandtl number on Nusselt number, RWP, $\beta = 45°$, $L = 3.75\ H$, $h = 0.6H$, $l = 1.2H$, $Re = 1.5 \times 10^5$

Pr	0.1	0.7	3.5	7.0	20
Nu_0	82.6	351.3	1031	1517	2457
$\overline{Nu}/Nu_0$	5.25	3.41	2.81	2.63	24.6
f/f_0	32	32	32	32	32
P_{ROC}/P_{RO}	299	67.8	34.9	27.8	22.1

Table 5. Combined effect of rib-roughness and rectangular winglets, $e/H = 0.03$, $r/e = 10$, $L/H = 3.75$, $h = 0.6H$, $l = 1.2H$, $Pr = 0.7$, $Re = 1.5 \times 10^5$

β	15°	25°	35°	45°
$\overline{Nu}/Nu_0$	3.29	3.73	4.14	4.46
$Nu_0 = 351.3$				
f/f_0	11.23	18	26.3	44
P_{ROC}/P_{RO}	35.6	51.9	71	88.7

The flow loss for an enhancement without vortex generators and roughness will be twice as high as with VGs and roughness.

4. CONCLUSION

A combination of longitudinal vortex generators on one wall and roughness elements on the other wall shows good potential for heat transfer enhancement. Average heat transfer enhancement of 450% can be obtained by this arrangement for the geometry and Reynolds number that have been investigated. Further studies are needed for the geometrical optimization of the winglet. We do not report the flow and heat transfer in a channel with VGs on both wall, since preliminary computations showed that the flow loss due to blockage could be several hundred times the plane channel flow.

REFERENCES

1. R. L. Webb, E. R. G. Eckert and R. G. Goldstein, Heat transfer and friction in tubes with repeated-rib roughness, *Int. J. Heat Mass Transfer* **14,** 601–617 (1971).
2. J. C. Han, L. R. Glicksman and W. M. Rolehnow, An investigation of heat transfer and friction for rib-roughened surfaces, *Int. J. Heat Mass Transfer* **21,** 1143–1156 (1978).
3. M. Fiebig, P. Kallweit, N. K. Mitra and S. Tiggelbeck, Heat transfer enhancement and drag by longitudinal vortex generators in channel flows, *ETF Sci.* **4,** 103–114 (1991).
4. St. Tiggelbeck, N. K. Mitra and M. Fiebig, Experimental investigations of heat transfer enhancement and flow losses in a channel with double rows of longitudinal vortex generators, *Int. J. Heat Mass Transfer* **36,** 2327–2337 (1993).
5. M. Fiebig, U. Brockmeier, N. K. Mitra and Th. Güntermann, Structure of velocity and temperature fields in laminar channel flows with longitudinal vortex generators, *Numer. Heat Transfer, Part A* **15,** 281–302 (1989).
6. J. X. Zhu, M. Fiebig and N. K. Mitra, Comparison of numerical and experimental results for a turbulent field with a longitudinal vortex pair, *J. Fluids Engng* **115,** 270–274 (1993).
7. J. X. Zhu, N. K. Mitra and M. Fiebig, Effects of longitudinal vortex generators on heat transfer and flow loss in turbulent channel flows, *Int. J. Heat Mass Transfer* **36,** 2339–2347 (1993).
8. W. R. Pauley and J. K. Eaton, Experimental study of the development of longitudinal vortex pairs embedded in a turbulent boundary layers, *AIAA J.* **26,** 816–823 (1988).
9. J. X. Zhu, Wärmeübergang und Strömungsverlust in turbulenten Spaltströmungen mit Wirbelerzeugern, Dissertation Ruhr-Universität Bochum, VDI Fortschrittberichte, Reihe 7, No. 192 (1991)
10. B. E. Launder and D. B. Spalding, The numerical computation of turbulent flows, *Comput. Meth. appl. Mech. Engng* **3,** 296–289 (1974).
11. K. Hanjalic and B. E. Launder, Fully developed asymmetric flow in a plane channel, *J. Fluid Mech.* **51,** Part 2, 301–335 (1972).
12. M. D. Donne and L. Meyer, Turbulent convective heat transfer from rough surfaces with two-dimensional rectangular ribs, *Int. J. Heat Mass Transfer* **20,** 583–620 (1977)
13. C. W. Hirt, B. D. Nichols and N. C. Romero, SOLA—a numerical solution algorithm for transient fluid flows, Los Alamos Scientific Laboratory Report LA- 5652, Los Alamos (1975)
14. S. Kakac, R. K. Shah and W. Aung, *Handbook of Single Phase Convective Heat Transfer*, pp. 3–42. Wiley, New York (1987).
15. E. M. Sparrow, J. R. Lloyd and C. W. Hixon, Experiments on turbulent heat transfer in an asymmetrically heated rectangular duct, *J. Heat Transfer* **88,** 170–174 (1966).